The East Greenland Coastal Current: Structure, variability, and forcing

David A. Sutherland[1*] and Robert S. Pickart[2]

[1] *MIT-WHOI Joint Program in Physical Oceanography*
Woods Hole Oceanographic Institution
360 Woods Hole Road, MS #21
Woods Hole, Massachusetts, USA 02543

[*] *corresponding author, email: dsutherland@whoi.edu*
tel: 508-289-3803 fax: 508-457-2181

[2] *Department of Physical Oceanography*
Woods Hole Oceanographic Institution
360 Woods Hole Road, MS #21
Woods Hole, Massachusetts, USA 02543

Accepted in *Progress in Oceanography*
March 2008

Abstract

The subtidal circulation of the southeast Greenland shelf is described using a set of high-resolution hydrographic and velocity transects occupied in summer 2004. The main feature is the East Greenland Coastal Current (EGCC), a low-salinity, high-velocity jet with a wedge-shaped hydrographic structure characteristic of other surface buoyancy-driven currents. The EGCC was observed along the entire Greenland shelf south of Denmark Strait, while the transect north of the strait showed only a weak shelf flow. This observation, in conjunction with water mass considerations and other supporting evidence, suggests that the EGCC is an inner branch of the East Greenland Current (EGC) that forms south of Denmark Strait. It is argued that bathymetric steering is the most likely reason why the EGC apparently bifurcates at this location. Repeat sections occupied at Cape Farewell between 1997 and 2004 show that the alongshelf wind stress can have a strong influence on the structure and strength of the EGCC and EGC on timescales of 2-3 days. Accounting for the wind-induced effects, the volume transport of the combined EGCC/EGC system is roughly constant (~2 Sv) over the study domain, from 68°N to Cape Farewell near 60°N. The corresponding freshwater transport increases by roughly 60% over this distance (59 to 96 mSv, referenced to a salinity of 34.8). This trend is consistent with a simple freshwater budget of the EGCC/EGC system that accounts for meltwater runoff, melting sea-ice and icebergs, and net precipitation minus evaporation.

Keywords: coastal currents, East Greenland current, sea ice, boundary currents, Arctic freshwater flux

Regional terms: subpolar North Atlantic, East Greenland, Cape Farewell

1

1 Introduction

Renewed interest in the circulation of high latitude shelves has arisen due to the important role that freshwater fluxes seem to play in controlling regional ocean circulation and, ultimately, global climate variability (e.g., Bryan, 1986; Aagaard and Carmack, 1989; Curry et al., 2003; Dickson et al., 2007). For example, coastal currents such as the buoyancy-driven Norwegian Coastal Current or the Alaskan Coastal Current are believed to influence strongly the regional freshwater budgets of their respective shelves (Mork, 1981; Weingartner et al., 2005). However, many aspects by which freshwater is transported within the polar and subpolar seas remain unclear, including the manner in which such coastal flows interact with the basin scale circulation. While small-scale river plumes have received considerable attention (e.g., Lentz and Largier, 2006; Yankovsky and Chapman, 1997), freshwater on the subpolar shelves is input from numerous sources, including melting sea ice, meltwater runoff from the mainland, and precipitation, resulting in coastal currents that are significantly broader than individual river plumes (e.g., Weingartner et al., 1999; Fong et al., 1997).

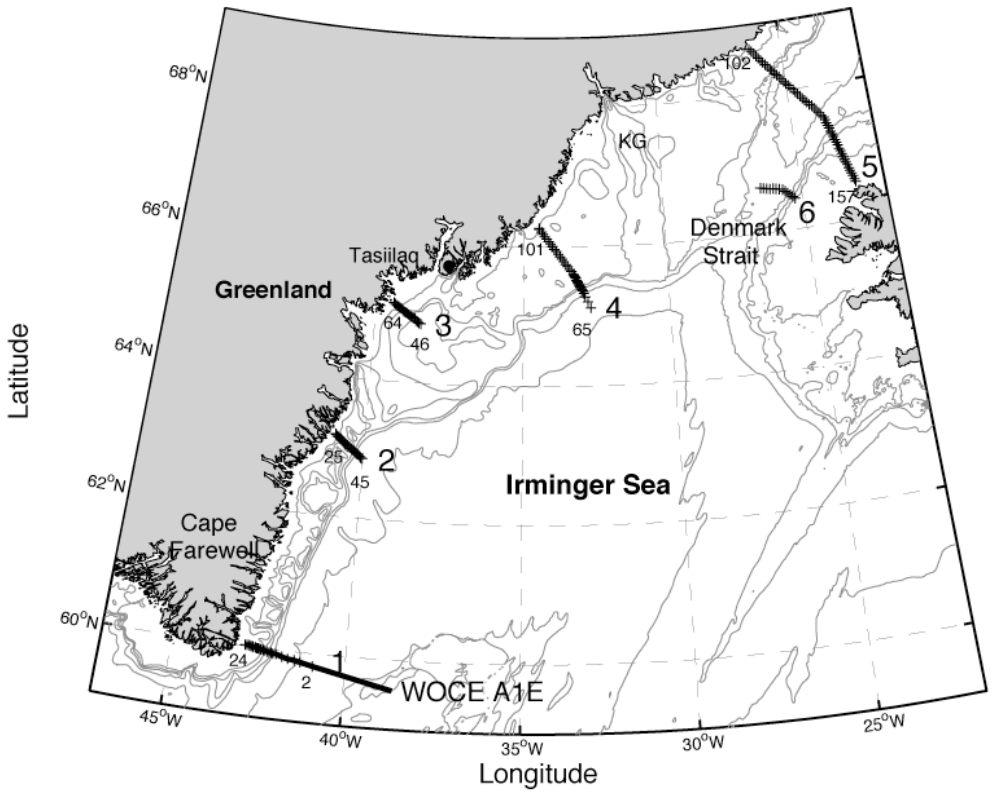

Figure 1. Map of JR105 station locations (+ symbols) and the WOCE A1E transect (solid line) off Cape Farewell. The 200, 350, 500, 1000, 2000, and 3000 m isobaths from the GEBCO bathymetric database are shown in light grey (IOC et al., 2003). Large numbers refer to JR105 sections, while the smaller numbers identify individual stations. KG denotes the location of the Kangerdlugssuaq Trough.

In the region of southeast Greenland (Fig. 1), the Arctic-origin, low-salinity East Greenland Current (EGC) flows southward along the shelfbreak next to the Atlantic-origin, high-salinity Irminger Current (IC). The combined transport of the EGC, the IC, and the Deep Western Boundary Current is one measure of the subpolar gyre strength, with previous estimates in the range of 27–36 Sv (e.g., Clarke, 1984; Bacon, 1997; Pickart et al., 2005). Inshore of the EGC and IC, on the inner-shelf, a wedge of low-salinity water has been observed trapped against the coast. Using vessel-mounted acoustic Doppler current profiler data and two hydrographic stations collected near Cape Farewell during the summer of 1997, Bacon et al. (2002, hereafter B02) determined that this feature was associated with a southward-flowing jet, which they named the East Greenland Coastal Current (EGCC). The transport of the EGCC was calculated to be ~0.8 Sv, and B02 suggested that it was mainly a seasonal feature resulting from coastal runoff.

In 2001 the same feature was sampled with higher resolution hydrographic measurements and was reported to transport 2 Sv of water (Pickart et al., 2005). This volume flux is surprisingly large, on the same order of the 1-2 Sv carried by the EGC in the vicinity of Denmark Strait (Hansen and Østerhus, 2000). Furthermore, using the data from the Pickart et al. (2005) study, the associated freshwater transport of the EGCC (referenced to a mean salinity of $S = 34.956$) is 57 mSv - almost 50% of the annual mean freshwater export from the Arctic Ocean through Fram Strait (Aagaard and Carmack, 1989; Dickson et al., 2007). Although this is a synoptic estimate, 57 mSv equals about four times the mean Alaska Coastal Current freshwater transport of 400 km^3/yr (31.54 $km^3/yr \approx 1$ mSv $= 10^3$ m^3/s), which constitutes a large fraction of the freshwater entering the Arctic Ocean through Bering Strait (Woodgate and Aagaard, 2005).

Prior to B02's study, there were other sparse measurements of the flow along the inner East Greenland shelf. The oldest such observations date back to the joint Icelandic-Norwegian cruises of the 1950's and 1960's reported by Malmberg et al. (1967). Using geostrophic velocities referenced with current meter data from shelf moorings, they found a transport of 1.6 Sv for the EGCC, although they referred to it as the East Greenland Current (Malmberg et al., 1967). A recent review of these and other historical CTD data clearly confirm the presence of the EGCC along the southeast coast of Greenland (Wilkinson and Bacon, 2005). When the surface 33.5 isohaline is used as a proxy, the EGCC appears to follow the 500 m isobath (Wilkinson and Bacon, 2005). However, low

surface salinities do not necessarily represent solely the EGCC feature, but could suggest the presence of melting sea ice that occurs along the path of EGC and IC. More recent drifter studies are consistent with the notion of a two-branched system on the East Greenland shelf, with one southward velocity core close to shore corresponding to the EGCC, and the other at the shelf break presumably associated with the EGC and IC (Reverdin et al., 2003; Jakobsen et al., 2003).

Despite the growing interest in the EGCC, and the available historical data, many basic questions remain about this current. For example, if the EGCC does exist north of Cape Farewell, as implied from historical and drifter data, what is its origin and how does it evolve equatorward? Is the EGCC actually a distinct feature from the EGC and, if so, how does it compare to other high-latitude coastal currents? Are the dynamics setting the horizontal and vertical scales of the EGCC similar to those controlling the behavior of smaller scale river plumes? Questions such as these motivated a field program undertaken in summer 2004, to investigate the EGCC south of Denmark Strait. This was the first high-resolution survey of the coastal current (station spacing on the order of 5 km), and was carried out using an icebreaker. The main goal of the cruise was to establish the existence of the coastal current and determine to what extent it was driven by coastal runoff (as surmised by B02).

The paper is organized as follows. The field program is described in section 2, while the remainder of the paper addresses the questions posed above. Section 3 presents the vertical sections collected in 2004 and shows that, indeed, the EGCC is present along the entire southeast Greenland shelf. In section 4 we investigate how the volume and freshwater transport of the EGCC varies along the shelf. To better understand these transport trends, the temporal and alongstream variability of the current are examined in sections 5 and 6, respectively, using not only the 2004 data, but observations from 2001-2003 as well. We then compute a freshwater budget of the EGCC in section 7 that accounts for meltwater runoff, melting sea-ice and icebergs, and net precipitation minus evaporation. Finally, we discuss the implications of our results in section 8 and present a new summertime circulation scheme for the southeast Greenland shelf.

2 Data and Methods

2.1 Data collection

The main source of data for this study comes from a July-August 2004 cruise on the ice-strengthened vessel *RRS James Clark Ross* (JR105) along the transects shown in Fig. 1. Six sections were occupied with a total of 170 hydrographic stations taken at high cross-stream resolution (3-5 km), with a Seabird 911+ conductivity/temperature/depth (CTD) system. Water to measure dissolved oxygen, salinity, and nutrient concentrations was obtained with a 12 x 10 liter bottle rosette. The salinity bottle data were used to calibrate the CTD conductivity sensor (accuracies are 0.002 for salinity and 0.001°C for the temperature sensor). A shipboard thermosalinograph continuously recorded surface temperature and salinity along the ship track. Velocity measurements were obtained with a narrow-band, 150 KHz vessel-mounted acoustic Doppler current profiler (ADCP) that ran continuously during the cruise.

A key advantage of this data set is the high-resolution station spacing and the relative proximity to the coast of each inshore station (both on the order of 5 km). This represents the first oceanographic data of its kind for the southeast Greenland inner shelf between Denmark Strait and Cape Farewell. We also have high-resolution data from transects taken in the summers of 2001-2003 by the *R/V Oceanus* (OC369 in 2001, OC380 in 2002, and OC395 in 2003) on the western end of the World Ocean Circulation Experiment (WOCE) A1E line off Cape Farewell (Fig. 1). These data were collected and processed identically to the JR105 data discussed here.

2.2 Hydrographic data processing

The CTD station data, consisting of salinity (S) and temperature (T), were pressure averaged to a resolution of 2 db. We then constructed vertical property sections by interpolating the data onto regular grids, with a resolution of 3 km in the horizontal and 10 m in the vertical, using a Laplacian-spline interpolation scheme. Potential density (σ_θ) and potential temperature (θ) fields, referenced to the sea surface, were constructed from the gridded sections. Most of the CTD stations attained a maximum depth of less than 5 m from the bottom. The bottom topography for the portion of the sections extending from the inshore-most station to the Greenland coast was interpolated from the General Bathymetric Chart of the Oceans (GEBCO) one-minute gridded bathymetric data set (IOC et al., 2003).

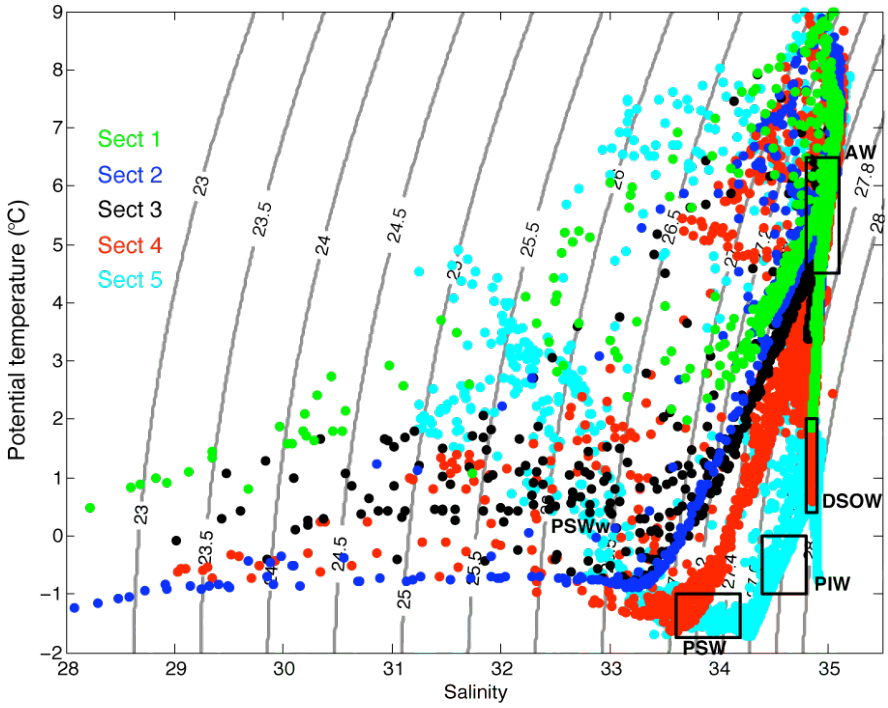

Figure 2. *θ*/*S* diagram for the entire JR105 data set, distinguished by section (see key). Irminger Sea and southeast Greenland shelf water mass definitions are: Atlantic Water (AW), Polar Surface Water (PSW), Denmark Strait Overflow Water (DSOW), Polar Intermediate Water (PIW), and warm Polar Surface Water (PSWw). See text for discussion and specific water type property ranges.

2.3 Velocity data processing

Absolute geostrophic velocity sections were constructed using the gridded σ_θ fields along with the concurrent ADCP measurements as outlined below. Prior to this the barotropic tidal signal was estimated and subtracted out of the ADCP data using the Egbert et al. (1994) tidal model (TPXO6.2). Errors associated with the detiding procedure come largely from inaccuracies in the bathymetric data available for the Greenland shelf, so tidal velocities there may be biased by several cm/s (Sutherland, 2008). This is small compared to the signals of interest in the EGC and EGCC, which are O(50 cm/s). Although care was taken in trying to sample perpendicularly across the main jet features on the shelf and slope (whose mean path should parallel the isobaths), maximum velocity vectors were sometimes oriented at an angle to the transect line. By rotating each velocity section into a streamwise coordinate system, any bias associated with how the current changes its orientation with respect to the bathymetry is minimized (see Halkin and Rossby, 1985; Fratantoni et al., 2001). Such a coordinate transformation was applied to the JR105 ADCP data following the steps outlined by Fratantoni et al. (2001). Care was

taken to keep the observed jet features on the shelf (the EGCC) and over the slope (the EGC/IC system) separate in the processing.

The de-tided and rotated ADCP velocities were interpolated onto the same regular grid as the hydrographic variables. Surface ADCP bins were excluded, and the maximum depth of observations was either 400 m or 85% of the total bottom depth. Absolute geostrophic velocities in the alongstream direction, U_{abs}, were calculated by combining the thermal wind velocities, U_g, with the alongstream ADCP velocities, U_{adcp}. In particular, the average of U_{adcp} and U_g over the depth range of available ADCP data were matched at each horizontal grid point, such that

$$U_{abs}(x,z) = U_g(x,z) + U_{ref}(x). \quad (1)$$

The reference velocity, U_{ref}, is defined to be

$$U_{ref}(x) = \frac{1}{h}\int_h U_{adcp}(x,z)dz - \frac{1}{h}\int_h U_g(x,z)dz \quad (2)$$

where h is the water column depth, and x,z are the cross-stream, vertical distances. In all of the JR105 sections $U_{ref} \neq 0$, indicating the presence of barotropic effects. This implies that using solely the relative velocities would inaccurately estimate the speed of both the EGCC and EGC. Throughout the rest of the paper, we refer to U_{abs} simply as the velocity and define other velocities as they are needed.

3 Hydrographic and velocity structure

Several previous studies have documented the θ/S properties of waters near the East Greenland shelfbreak and their alongshelf evolution (e.g., Krauss, 1995; Rudels et al., 2002). On the offshore side of the EGC/IC system resides a water mass historically referred to as Irminger Sea Water (Clarke, 1984) with approximate θ/S properties of 4-5°C and $S \sim 35$. This is believed to be a product of mixing between the EGC and IC, influenced as well from heat loss due to intense atmospheric forcing during the winter months. In the interior of the basin lies Northeast Atlantic Water, a Gulf Stream remnant water with $\theta > 7$°C and $S > 35$, that has undergone little modification since first entering the region along the Reykjanes Ridge as part of the northward-flowing Irminger Current. For simplicity in this paper, we combine the two Atlantic-influenced water masses into a single, saline Atlantic Water (AW) type identified in Fig. 2 with $\theta \sim$ 4.5-6.5°C and $S \sim$ 34.8-35.1.

The cold, fresh waters near the shelfbreak and on the shelf originally derive from the Arctic and can be classified into three water masses: Polar Intermediate Water (PIW), Polar Surface Water (PSW), and warm Polar Surface Water (PSWw) (Rudels et al., 2002). PIW is the densest of these, defined as water with $\sigma_\theta > 27.70$ and $\theta < 0°C$ that comes from the colder parts of the Arctic Ocean thermocline. PSW is lighter with $\sigma_\theta < 27.70$, but can be very cold, with $\theta < 0°C$. Melting sea ice warms and freshens this PSW, which also warms slightly on its way south due to air-sea interaction. This transformed water mass, PSWw, can exhibit a range of θ/S properties depending on the processes modifying it, although in general PSWw is lighter than PSW and warmer than $\theta > 0°C$, as shown in Fig. 2.

3.1 Defining the EGCC

To obtain an objective definition of the EGCC we utilize not only the θ/S properties and water masses described above, but also present vertical sections of the hydrographic properties and velocity from JR105. We emphasize this descriptive aspect of the study since previous studies, based on sparser data, could not consistently distinguish between the EGCC and the EGC.

Numerous definitions have been used in the past to delineate the EGC based on hydrography: Pickart et al. (2005) used the 34.9 isohaline to distinguish the EGC from the IC, while Nilsson et al. (2006) considered just the freshest part of the EGC using $S < 34.5$ as an EGC delimiter. Older studies also commonly focused on the freshest part of the EGC only ($S \sim 34\text{-}34.9$), if the current was distinguished from the IC at all (Clarke, 1984; Krauss, 1995). In retrospect, some of these studies were probably considering part of the EGCC and not recognizing its distinct nature from the EGC. Using these past studies as a guide, we use the 34.8 isohaline to mark the boundary between the EGC and IC.

Objectively defining the EGCC as a distinct feature from the EGC is a separate issue, since their salinity ranges can overlap. In this study we use a combination of velocity and salinity to distinguish the two currents. Specifically, we define the lateral limits of the EGCC by where the velocity decreases to 15% of the maximum inner jet velocity. This defines the width scale, w_{obs}, of the observed current. The depth scale, h_{obs}, is taken to be where the 34-isohaline intersects the bottom near the coast. For example, at Cape Farewell the EGCC is delimited by the inner green box in Fig. 3, with $w_{obs} = 30$ km

and h_{obs} = 75 m. Similarly, the EGC is delimited by the outer green box, which is drawn according to both the velocity and salinity criteria noted above. The boxes are meant only as guides to show where the salinity and velocity criteria are used to delineate the EGC from the IC and the EGCC. Transports and freshwater fluxes, as well as the depth and width scales of the two currents, are computed using the gridded data that satisfy these specific velocity and salinity criteria.

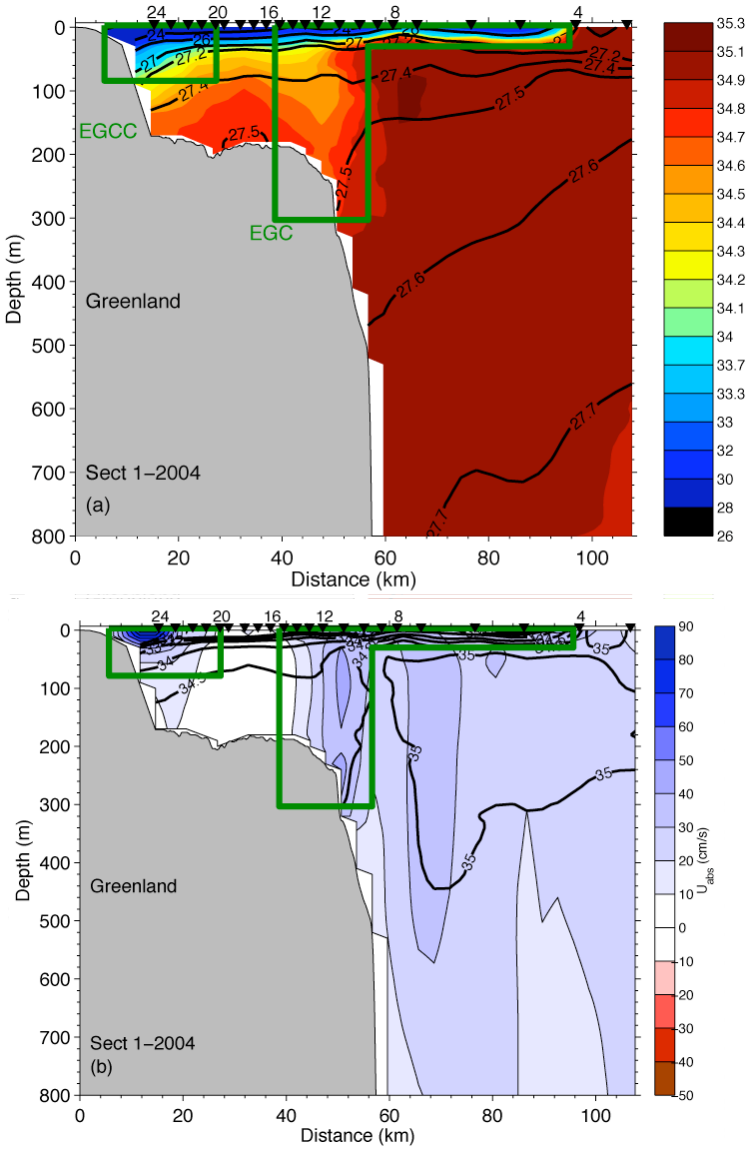

Figure 3. *(a)* Salinity field (color) from 2004 JR105 section 1 near Cape Farewell (60°N) with select isopycnals (kg/m^3) contoured in black. Boxes outline the boundaries defined in the text for the EGCC and the EGC. Black triangles mark the numbered CTD stations. *(b)* Alongstream absolute velocity, U_{abs} (color, cm/s), for 2004 JR105 section 1 where U_a > 0 denotes equatorward flow. The isohalines (34, 34.5, 34.8, and 35) used in defining the currents are contoured in black.

Vertical sections of salinity and velocity for all the JR105 transects, displayed in Fig. 3-7, are the best indicators of the current; these two fields are shown in relation to each other to illustrate the basic structure of the EGCC. Temperature, although an important identifier of water masses, plays a minor role in controlling the density of the upper-layer boundary currents in this subpolar region.

Section 1 – Cape Farewell (60°N)

Fig. 3a displays the salinity field for the southern-most transect near Cape Farewell, a good starting place to facilitate comparison with previous studies regarding the characteristics of the EGCC. First, the sharp salinity front near station 11 separating fresh polar-origin water and salty Atlantic-influenced water is the EGC/IC front, although the surface expression of the front is found 40 km farther offshore. The near vertical isohalines distinguish the AW in the IC from the EGC waters with $S < 34.8$. No PSW exists this far south, as it has been modified extensively along the path of the current, becoming PSWw as shown in Fig. 2.

Inshore of station 20, a wedge of very fresh water, $S < 32$, lies over the shelf roughly 20 km shoreward of the EGC/IC front. This is the front associated with the EGCC. The 34-isohaline descends to a depth of about 75 m at the coast, which is much shallower than observed in 2001 when $h_{obs} \approx 110$ m (Pickart et al., 2005), or in 1997 where observations showed no water with $S > 34$ at the innermost CTD station (B02). Another feature seen only in 2004 is the low-salinity surface waters that extend seaward from the shelfbreak with an average depth of about 10 m. This is roughly the mixed layer depth (defined as the depth where σ_θ exceeds 0.125 kg/m^3 of the surface value), suggesting the important influence of wind and/or other mixing processes to the EGCC and EGC. This feature also implies that using surface hydrographic or satellite data to infer the position of the EGCC can be misleading, since in this case the 34-isohaline outcrops almost 100 km from the coast, while the two currents are actually found much closer inshore. Mixed layer depth estimates in the region just offshore (seaward of station 4) of this fresh, surface cap are much deeper (~60 m).

Associated with the low salinity wedge on the inner shelf is a distinct equatorward jet, with maximum velocities > 90 cm/s and significant flow throughout the water column. This is the EGCC, although we did not cross the entire current and hence extrapolation was necessary to obtain volume and freshwater transport values of the

current at this location (see below). A region of very weak flow separates the EGCC from the EGC velocity core centered near the salinity front at station 11. Offshore of the EGC near station 7 is a deep-reaching equatorward flow that likely corresponds to the IC. In previous studies, the IC and EGC were reported as a merged system in velocity, though they were easily distinguished in θ/S space (Pickart et al., 2005). In 2004, the two currents seem to be distinct in their velocity signals as well.

Section 2 – Near 63°N

Section 2 is located approximately 350 km farther to the north, on the narrowest part of the southeast Greenland shelf at 63°N (Fig. 1). Again, a wedge of fresh water dominates the salinity structure in Fig. 4a over the shelf, although it is much deeper at the coast ($h_{obs} \approx 200$ m) than the wedge observed at Cape Farewell. The water found here contains a strong core of PSW. The influence of warm, salty water is still present though, with the eroded PSW core on a mixing line with AW (Fig. 2). The EGC/IC front at this section is located near stations 37-38. Inshore of this front, the mixed layer depth is deeper than observed at section 1, ranging from 10-20 m, but still shallower than offshore where the average mixed layer depth is ~50 m. The EGCC at this section is quite pronounced, with maximum velocities near the surface exceeding 100 cm/s and near-bottom values up to 30 cm/s (Fig. 4b). Near the shelfbreak it is difficult to isolate the EGC compared to the distinct signature seen at Cape Farewell. The confusion in nomenclature between the EGCC and EGC is most evident here, since many previous investigators would refer to the flow on the shelf as the EGC, while we reserve that for the shelfbreak portion alone. Bathymetry may play a part in this as the shelf is very narrow here (about 40 km wide versus > 100 km farther north), thus bringing the EGC and EGCC flows together. The enhanced equatorward flow on the slope (centered at 500m) is likely the East Greenland Spill Jet discussed by Pickart et al., (2005).

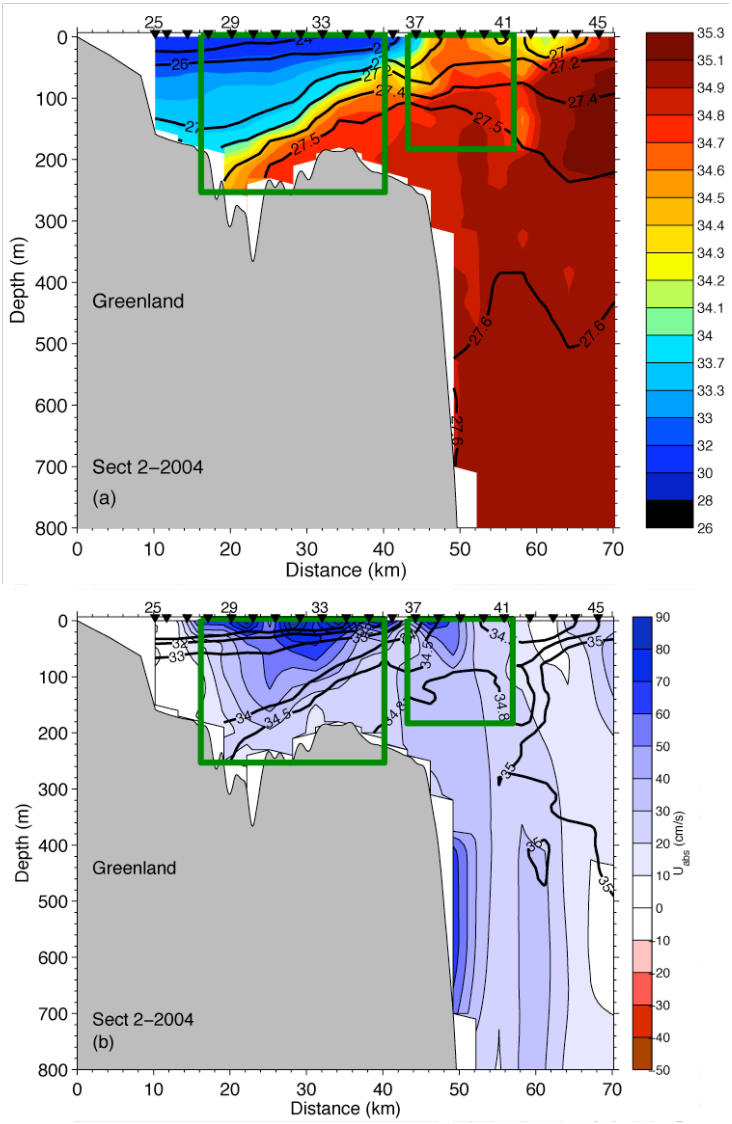

Figure 4. Same as Fig. 3, except for 2004 JR105 section 2, which is near 63°N.

Section 3 – Near 65°N

At this latitude the shelf contains an 800 m deep basin, and the JR105 section sampled only the inshore part of this basin (which extends very close to the coast), missing any shelfbreak flow. This implies that the current observed at section 3 is exclusively the EGCC, yet EGC influence cannot be ruled out since the basin extends out to the shelfbreak. An onshore diversion of part of the EGC here is supported by studies showing southward-directed drifter tracks on both sides of the basin (Reverdin et al., 2003; Jakobsen et al., 2003). As in the sections to the south, we observed a fresh wedge of water at this location indicative of the surface intensified EGCC, with a strength of 60 cm/s. The freshest water in Fig. 5a is again the coldest, falling in the PSWw regime,

although, unexpectedly, it is warmer than observed at section 2 (Fig. 2). Another surprise is the presence of salty water, $S > 34.8$, found in the subsurface waters near station 46, far inshore of the shelfbreak. This also supports the notion of flow being diverted toward the inner shelf, bringing with it AW influence from the EGC/IC system.

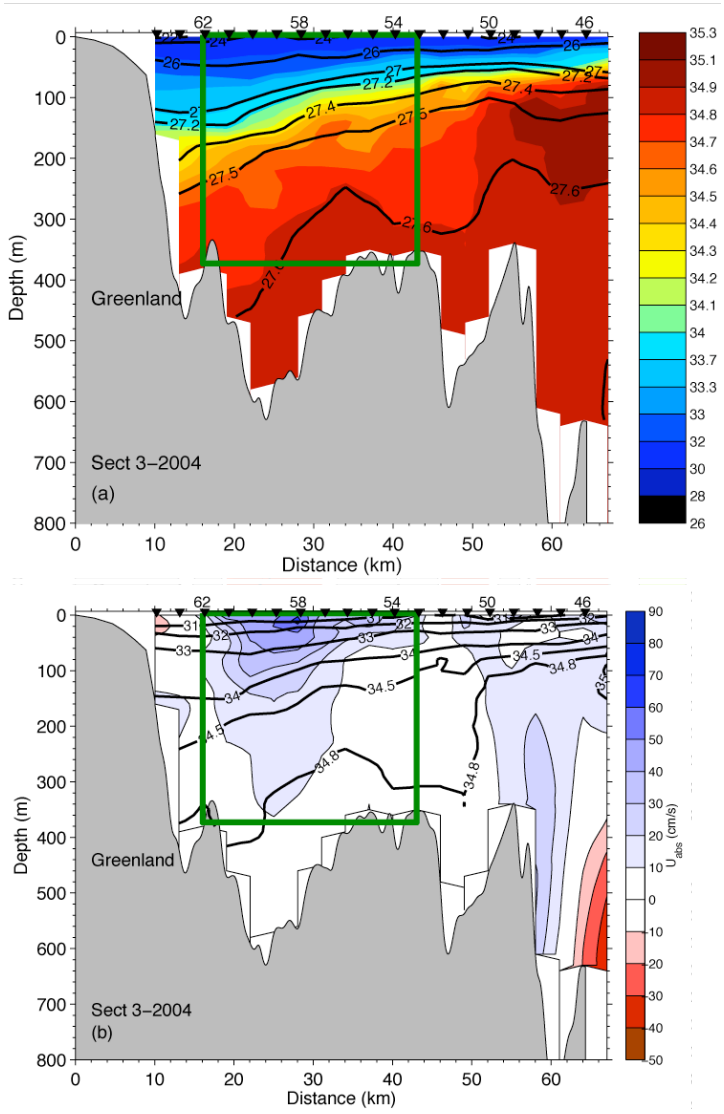

Figure 5. Same as Fig. 3, except for 2004 JR105 section 3, which is near 65°N.

Section 4 – Near 66°N

Section 4 lies north of Tasiilaq where the shelf reaches its widest point. The salinity field has a large wedge of fresh water over much of the shelf down to a depth of 150 m (Fig. 6a). Some low-salinity water also resides in the vicinity of the shelf break, yet the dominant features there are the two lenses of salty water, $S > 34.8$ (centered at stations 73 and 79 respectively), likely associated with AW eddies originating from the IC. Such features have been observed previously (Krauss, 1995; Rudels et al., 2002;

Pickart et al., 2005) and represent a source of AW reaching onto the shelf. The θ/S characteristics of the water at section 4 (Fig. 2) indicate the presence of pure PSW, some modified PSWw, and a strong AW influence. The densest water in the section is likely a combination of Denmark Strait Overflow Water (DSOW, a dense water mass with $\sigma_\theta >$ 27.8, $\theta > 0$°C and $S \sim$ 34.8-34.9), together with water from the Spill Jet.

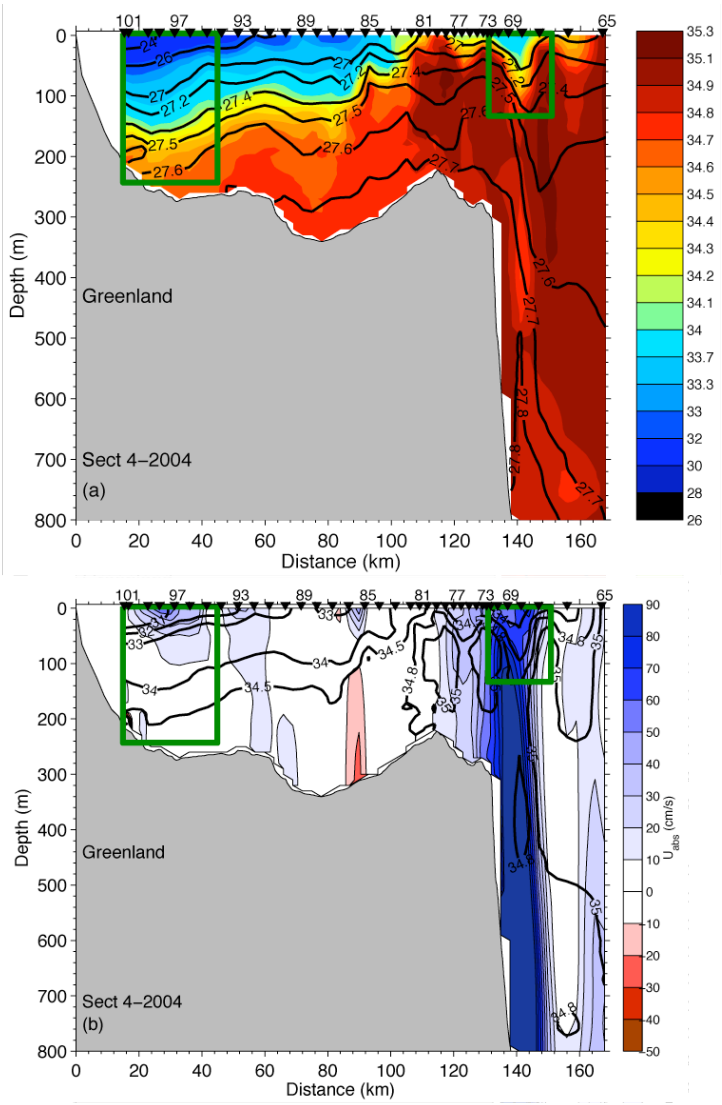

Figure 6. Same as Fig. 3, except for 2004 JR105 section 4, which is near 66°N.

The freshest and coldest water at section 4 is located on the inner shelf, shoreward of station 93, corresponding to a surface-intensified jet (Fig 6b). This sub-wedge of salinity ($S < 32$) corresponds to the EGCC, with a maximum velocity of ~ 60 cm/s. The previous studies of Malmberg et al. (1967) and Nilsson et al. (2006) sampled only sparsely near this location, and consequently resolved only the large-scale signature of the fresh wedge of water. Both studies referred to the corresponding flow as the EGC,

while the station spacing and closer proximity to the coast of the JR105 measurements indicate that the EGCC exists this far north as well. Note that the seaward edge of the fresh wedge, defined by the outcropping of the 34-isohaline near station 83, is not associated with a strong jet (Fig. 6b). This is another example of the care one must take when considering only surface data to describe the EGCC. In this section there is actually weak flow associated with most of the fresh wedge. By contrast, the EGC is confined to a shallow depth near the shelfbreak, centered near station 69 adjacent to the salty lenses noted above. The strongest flow in the section occurs on the slope near 500 m (near station 69), associated with the Spill Jet. The IC is usually observed at this latitude; we assume its absence is due to the limited offshore extent of the transect.

Section 5 – North of Denmark Strait (68°N)

Section 5 extended from the Greenland coast to the Icelandic coast, although we focus here on the northwestern portion of the transect only. The dominant feature of the salinity field (Fig. 7a) is the EGC front located near station 128. The isohalines descend about 200 m indicating the presence of the EGC in the middle of the basin upstream of Denmark Strait. The fact that the EGC is situated far offshore of the shelfbreak is not uncommon at this latitude; it has been observed detached from the shelfbreak previously and can re-attach downstream of the strait (Rudels et al., 2002). Water with $\sigma_\theta > 27.8$ kg/m^3 is usually associated with DSOW and this isopycnal is outlined in Fig. 7a. On the Greenland side of the EGC front, the water is lighter than this to about 300 m depth, indicating the presence of Arctic-origin surface waters. This is corroborated by the θ/S characteristics displayed in Fig. 2. Unmodified PSW and PIW exist at this latitude; the water lying in the AW range actually comes from the Icelandic Irminger Current flowing to the north adjacent to the Icelandic coast (not shown in Fig. 7).

Interestingly, even though the upper layer is fresh between the Greenland coast and the EGC front, there is no pronounced wedge akin to the sections farther south. Rather, there is only a slight overall tilt to the 34-isohaline from the EGC front towards Greenland to station 108. Embedded within this tilt is a small region of enhanced thermal wind shear and a weak maximum in velocity centered near station 114 (Fig. 7b). This is assumed to be the EGCC (Fig. 7b), with a maximum flow of ~30 cm/s and a depth of 200 m. By contrast, the EGC is very strong at this section, with a surface velocity exceeding 60 cm/s. Note the bowl-shaped structure of the deep isopycnals between stations 118 and

130. This corresponds to a recirculation over the deep basin with poleward flow on the western side. Whether or not this is a permanent feature is unknown, but it is clear that at the time of the survey not all of the observed EGC jet continued equatorward. Accordingly, we include the poleward part of the flow in defining the EGC and limit its depth extent to water with $\sigma_\theta < 27.8$ kg/m^3.

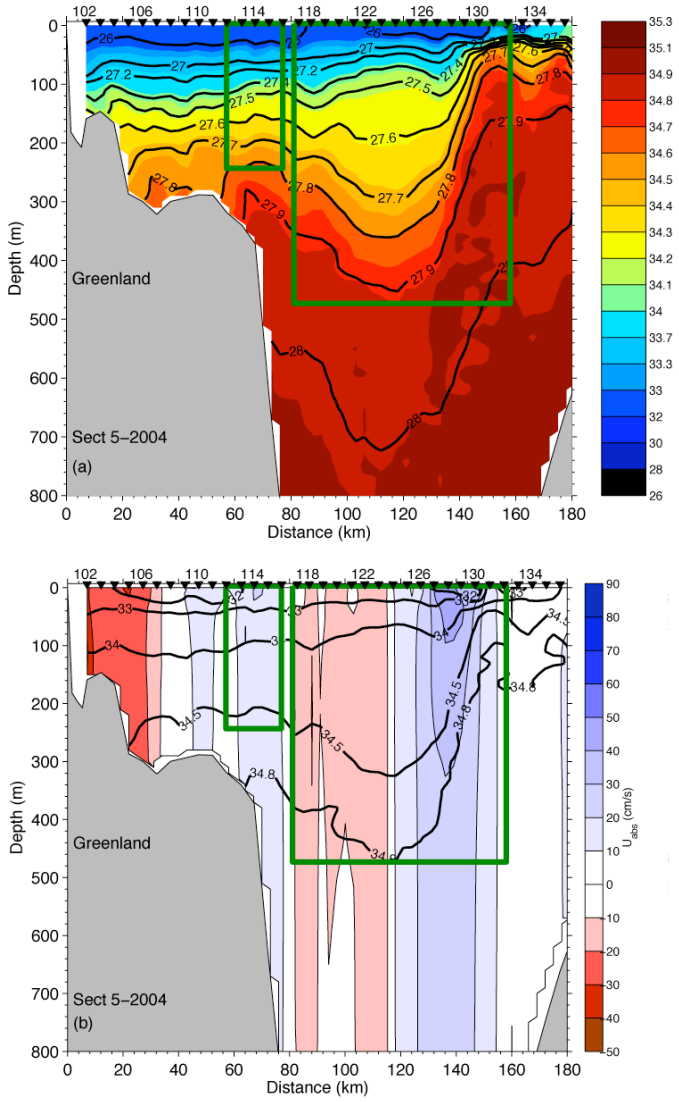

Figure 7. Same as Fig. 3, except for 2004 JR105 section 5, which is near 68°N.

4 Transports

4.1 Volume fluxes

Previous estimates of the EGCC volume transport range from 0.8–2.0 Sv at Cape Farewell (computed using vessel-mounted ADCP data; B02, Pickart et al., 2005), 1.6 Sv near JR105 section 4 (based on thermal wind shear referenced with current meters;

Malmberg et al., 1967), and a historical range of 0.2-2.0 Sv along the East Greenland shelf (from geostrophic calculations using the 33.5-isohaline as a guide, Wilkinson and Bacon, 2005). EGC transport estimates in the literature also exhibit a large range, depending on location, year, season of measurement, and how the current was defined. A transport budget of the Nordic Seas indicated that the EGC in Denmark Strait carries 1.3 Sv (Hansen and Østerhus, 2000). This value was used in a calculation for the Irminger Sea resulting in a transport of 0.7 Sv for the EGC south of Denmark Strait where the current merges with the IC (Pickart et al., 2005). Other transports reported for the EGC are larger and range up to 3.0 Sv (see the table in Pickart et al., 2005).

Volume transports calculated for each JR105 transect are shown in Fig. 8a. We include individual values for the EGCC and EGC, as well as the combined EGC/EGCC system, including error bars (for details on error estimates see Sutherland, 2008). We note that the ratio Q_a/Q_{geo} for the EGCC is generally > 1 (as large as 2 for the Cape Farewell section). The exception to this is at section 4 near 66°N where $Q_a/Q_{geo} \approx 0.5$, indicating the presence of a poleward barotropic flow at this location. Progressing equatorward, the EGCC synoptic transport increases roughly four-fold from section 5 north of Denmark Strait, where $Q_a = 0.48$ Sv to section 2 where $Q_a = 2.2$ Sv. An especially large increase occurs at section 2, followed by an abrupt decrease at Cape Farewell. The transport of the EGC through Denmark Strait is 1.1 Sv, within the published values (especially considering the strong recirculation observed there, Fig. 7). There is a decrease in volume flux at section 2 near 63°N. Interestingly, this is where the EGCC transport increases substantially, and when the two currents are considered as a single system, the anomalous nature of section 2 is reduced (but not completely removed). Other than this increase in total transport at section 2, the combined volume flux of the EGC/EGCC system remains approximately constant from north to south (1.6-1.9 Sv). Is there a convergence at section 2 or does this simply reflect the need for longer-term measurements since synoptic sections will inevitably exhibit variability? This question is discussed in section 5 where it is shown that the alongshelf wind stress can play an important role in modulating the EGCC transport.

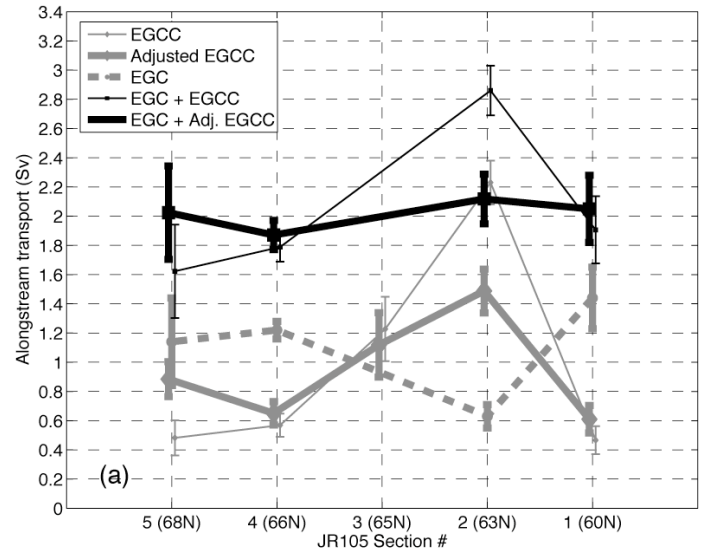

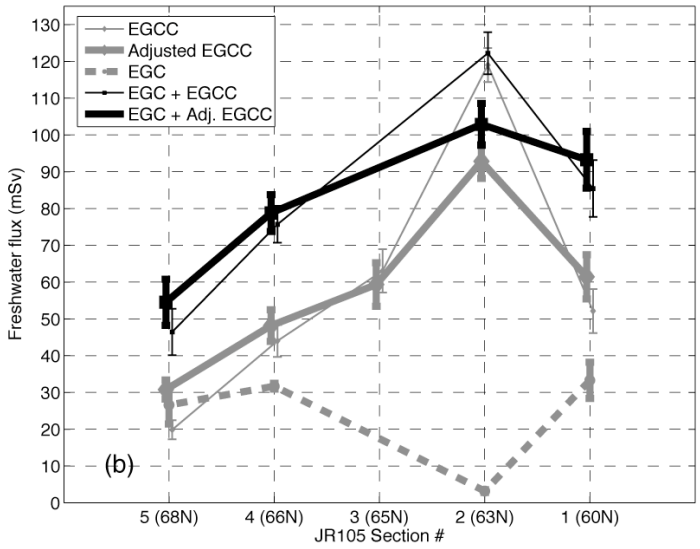

Figure 8. *(a)* Alongstream transport, Q_a (Sv), at each section for the currents on the East Greenland shelf: EGC, EGCC, and combined EGC/EGCC system. Definitions of the currents at each JR105 transect are given in the text. Thin lines show the original, unadjusted transports, thick lines show the wind-adjusted values. Note that no adjustment was done for the EGC data. *(b)* Same as *a* for the freshwater fluxes, FW_{flux} (mSv), at each JR105 section, with $S_{ref} = 34.8$.

4.2 Freshwater fluxes

Freshwater fluxes, as described below, are actually freshwater flux anomalies and are equivalent to the flux of zero salinity water that must be combined with a flux of water at a reference salinity to equal the observed flux at the observed salinity (Melling,

2000). The freshwater flux anomaly, FW_{flux}, is calculated as

$$FW_{flux} = \iint_{dzdx} U_{abs}(x,z) \cdot \frac{\left(S_{ref} - S(x,z)\right)}{S(x,z)} dxdz \qquad (3)$$

where U_{abs} is alongstream absolute velocity, S is the salinity, and $S_{ref} = 34.8$ is the reference salinity chosen to allow comparison with previous estimates of FW_{flux} (Aagaard and Carmack, 1989; Woodgate and Aagaard, 2005). Note that the B02 synoptic estimate of the EGCC FW_{flux} of 57 mSv was referenced to a mean salinity of 34.956, and it increases to ~66 mSv when $S_{ref} = 34.8$ is used.

Using the JR105 data, the EGCC FW_{flux} is calculated to be 52 mSv at Cape Farewell, similar in magnitude to the 1997 estimate of B02. Throughout the survey, however, the EGCC FW_{flux} estimates vary significantly (Fig. 8b). This is largely due to the variation in observed EGCC transports: the largest FW_{flux} of 119 mSv corresponds to the largest Q_a at 63°N (section 2). However, the salinity field does have a significant influence. For example, the volume transport at section 3 is almost twice that at Cape Farewell, but the freshwater flux of 63 mSv is not significantly different due to the very low salinities ($S < 28$) observed in the EGCC at Cape Farewell. Overall the FW_{flux} of the EGCC increases equatorward by 32 mSv. By comparison, Fig. 8b shows that the FW_{flux} of the EGC is relatively constant, 26–33 mSv, with the exception of section 2, where the current carries almost no freshwater ($FW_{flux} = 3$ mSv). As was true for the volume flux, this is the location where the EGCC FW_{flux} increases substantially, and considering the EGCC/EGC system together reduces the anomaly. The FW_{flux} of the EGC/EGCC system increases equatorward similar to the EGCC trend, since the EGCC FW_{flux} estimates are all greater than or equal to the EGC FW_{flux}. The net freshwater flux gain is about 39 mSv, although there is still a significant anomaly at section 2. Can the alongstream trend and net gain of freshwater in the JR105 data set be explained by available freshwater sources or by other variable forcing factors such as the wind? We examine this question further below.

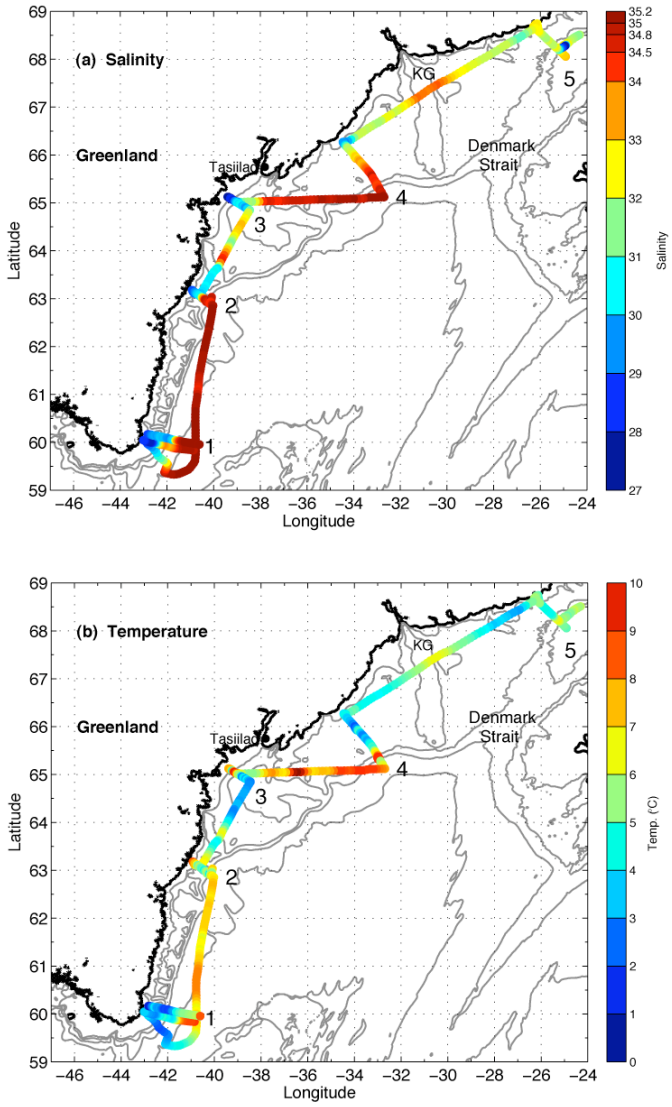

Figure 9. *(a)* Surface salinity field, *S*, from thermosalinograph data taken during JR105. The two lines near Cape Farewell are offset to allow visualization; one was taken during the CTD station work, while the other was taken coming offshore from Greenland. *(b)* Surface temperature field, *T* (°C), from thermosalinograph data taken during JR105.

5 Temporal variability of the EGCC/EGC system

As noted earlier, we observed a very fresh, $S < 32.5$, surface layer of water extending 100 km from the Greenland coast (Fig. 3a) in the JR105 CTD transect near Cape Farewell. This feature is present as well in the thermosalinograph data collected during the occupation of the transect (Fig. 9). Additional crossings of the shelf in the vicinity of Cape Farewell were made while mooring work was being carried out on the cruise. The thermosalinograph data from six days before the CTD transect shows that the $S < 32.5$ water was confined closer to the coast, completely inshore of the shelfbreak.

One possible explanation for this, as well as for the alongstream variability found in the above transport estimates, is forcing by the alongshelf winds. Fortunately, we can investigate the role of time varying winds on the EGCC at Cape Farewell since data were obtained in the three previous summers (2001-2003), as well as in summer 1997 (B02). To be complete, Figs. 10-12 display the salinity and alongstream velocity sections at Cape Farewell from 2001-2003. They are presented identically to the JR105 sections above.

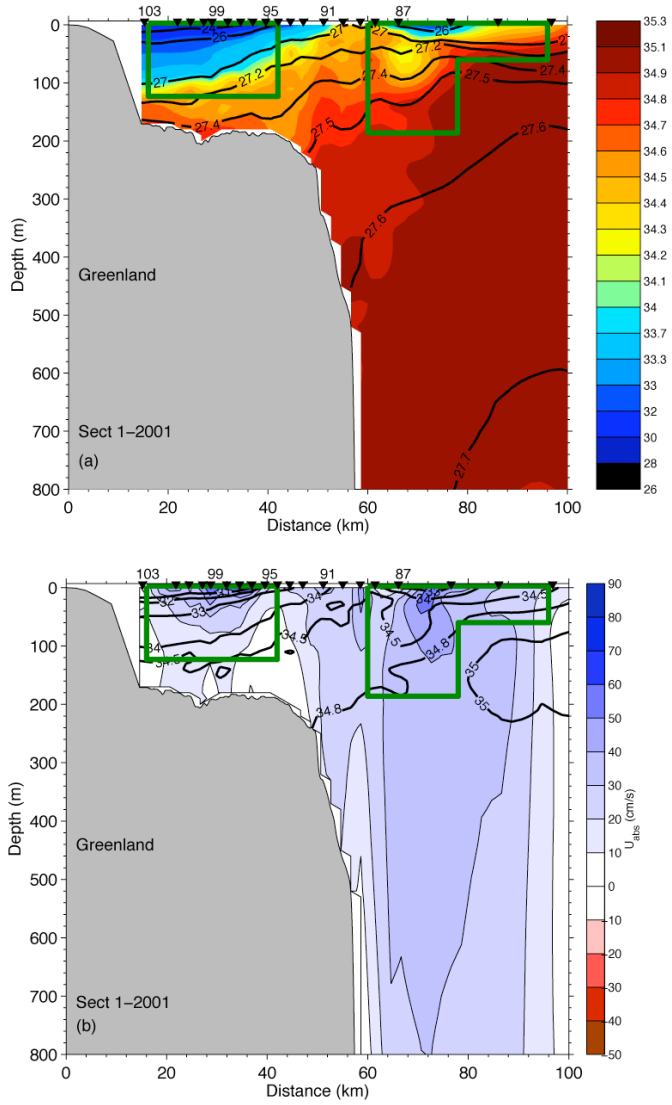

Figure 10. Same as Fig. 3, except taken in 2001 (OC369) near 60°N at Cape Farewell.

The first feature to note in comparing the different years' salinity fields is the pronounced variability in the depth of the 34-isohaline, which is used to determine the vertical scale of the EGCC front. In 2003 h_{obs} = 65 m, its shallowest value in all years, while in 2002 h_{obs} = 140 m. Overall it appears that in the summers of 2001-2004, the

EGCC at Cape Farewell was a surface-trapped buoyant current. To demonstrate this we compare the area of the current located offshore of the foot of the front to the area onshore, following Lentz and Largier (2006). The ratio of onshore area to offshore area, A_{on}/A_{off}, is << 1 for each section. Note that in 2003 the alongstream velocity of the EGCC is significantly greater than zero near the bottom (Fig. 12b). Hence the EGCC is not contained within the low-salinity wedge, as is true for the other occupations. However, even if the 34.5 isohaline is used to delimit the current in 2003, the ratio A_{on}/A_{off} is still < 1 (and this holds for each other year also), indicating that the EGCC is indeed surface-trapped.

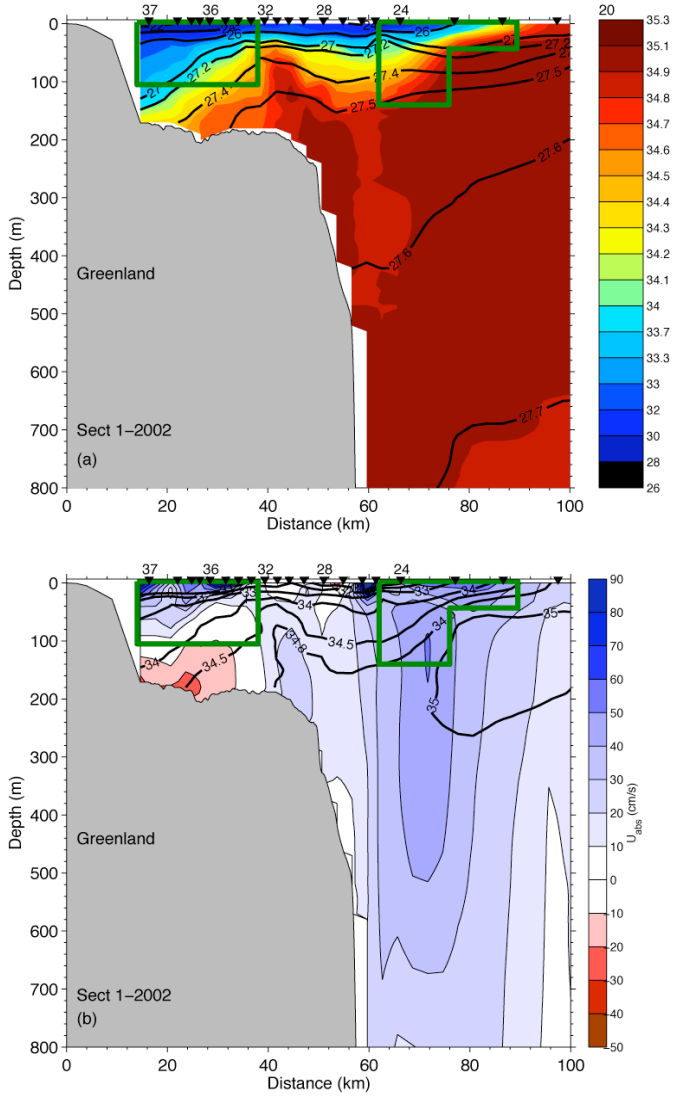

Figure 11. Same as Fig. 3, except taken in 2002 (OC380) near 60°N at Cape Farewell.

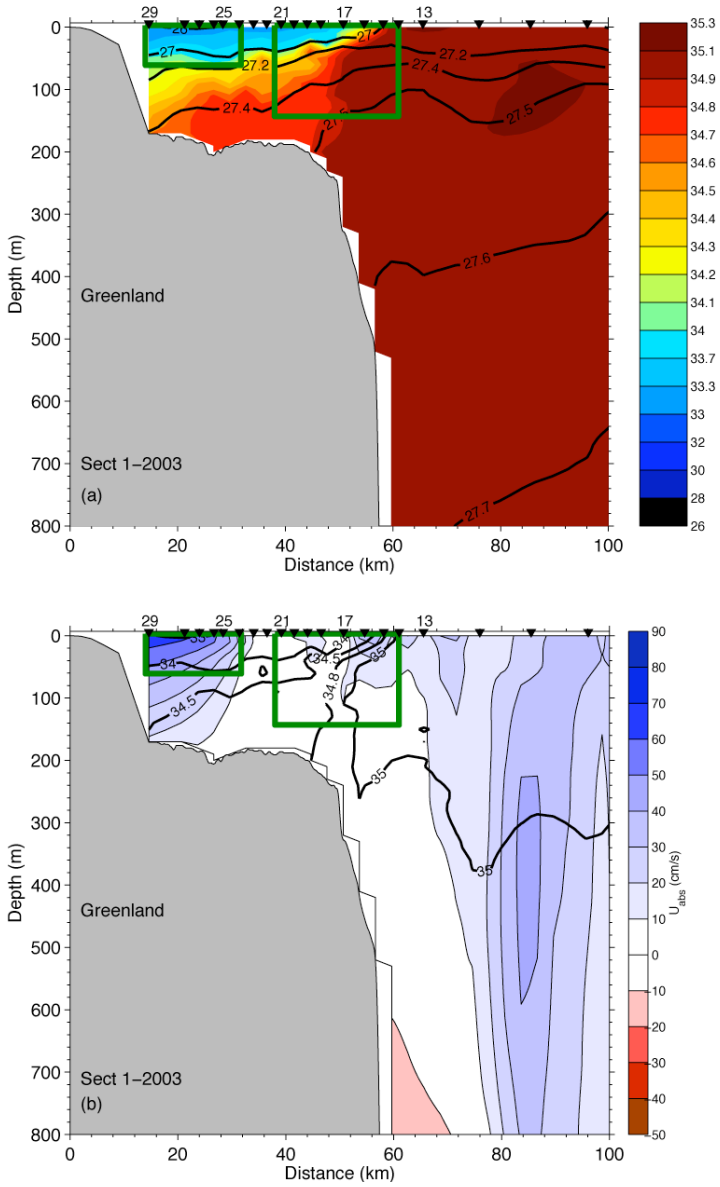

Figure 12. Same as Fig. 3, except taken in 2003 (OC395) near 60°N at Cape Farewell.

5.1 Dynamical scales of the coastal current

Numerous theoretical and observational studies have shown that alongshelf winds can influence a buoyant coastal current through an "Ekman straining" mechanism (e.g., Fong and Geyer, 2001; Lentz and Largier, 2006). Downwelling favorable winds steepen the front, tending to deepen and narrow the current as well as induce a barotropic velocity and reduce stratification within the current. Upwelling favorable winds shoal the foot of the front and widen the current through a thin mixed layer that moves offshore at a velocity that scales with the Ekman velocity. Theoretical estimates exist for the depth of the foot of the front, $h_p = (2Qf/g')^{1/2}$, and the width of the current, $w_p = (g' h_p)^{1/2}/f + w_b$,

where Q is the transport of the current, f is the Coriolis parameter, g' is the reduced gravity, and w_b is distance from the foot of the front to the coast (Yankovsky and Chapman, 1997). These estimates have been tested for smaller scale coastal currents, but never for a large-scale flow such as the EGCC. Previous studies have also attempted to separate the wind-driven and buoyancy-driven components of a coastal current by defining a wind strength index, $W_s = u_{wind}/u_{buoy}$ (Whitney and Garvine, 2005). W_s compares the wind-driven (u_{wind}) and buoyancy-driven (u_{buoy}) alongshelf velocity scales. If $|W_s| < 1$, the flow is in a buoyancy-driven state, whereas for $|W_s| > 1$, strong wind events dominate the flow.

Table 1. Ratios of the observed depth and width scales of the EGCC to theoretical scales, alongshelf wind stresses, and reduced gravities at Cape Farewell (JR105 section 1) from summer 1997, and 2001-2004. The scales are defined in the text, as is the wind strength index, W_s.

Year	h_{obs}/h_p	w_{obs}/w_p	τ_{along} [b] (N/m^2)	g' (m/s^2)	W_s
1997 (B02)	1.5	1.4	-0.027	0.038	-0.07
2001 (OC369)	1.4	1.1	-0.011	0.045	-0.13
2002 (OC380)	2.1	0.9	-0.016	0.055	-0.02
2003 (OC395)	0.6	0.9	-0.013	0.012	-0.50
2004 (JR105)	1.4	1.2	+0.022	0.045	0.15
2004 (JR105[a])	1.7	1.8	+0.026	0.045	0.09
2004 (JR105[a])	1.9	1.1	-0.010	0.045	0.03

[a] These data are based only on ADCP sections from crossings at Cape Farewell during JR105.
[b] Alongshelf wind stresses are 2-day averages, where $\tau_{along} < 0$ is downwelling favorable.

Table 2. Same as Table 1, but for the EGCC at sections north of Cape Farewell in 2004 (JR105).

Section	h_{obs}/h_p	w_{obs}/w_p	τ_{along} (N/m^2)	g' (m/s^2)	W_s
2 (63°N)	1.4	0.7	-0.028	0.037	-0.25
3 (65°N)	1.4	1.1	-0.008	0.037	-0.05
4 (66°N)	1.1	1.7	+0.012	0.037	0.13
5 (68°N)	N/A[a]	N/A[a]	+0.070	N/A[a]	0.25

[a] No estimates were made at this section due to the weak EGCC structure observed.

We estimate h_p and w_p using the computed alongstream transports, Q_a, reduced gravities, g', and the observed distances from the foot of the front to the coast, w_b. Ratios of the observed depth (h_{obs}) and width (w_{obs}) of the EGCC with the predicted depth and width scales all lie in the range 1-2 (see Table 1), with the 2003 data being the one exception. Note that in 2003 the depth of the 34-isohaline was shallow, although the equatorward flow extended much deeper (Fig. 12), which is why the predicted depth scale is greater than the observed. The transects north of Cape Farewell also behave qualitatively akin to what is expected. The ratios of observed depths and widths of the EGCC to the predicted scales are all O(1) as listed in Table 2. The most notable differences arise at section 2, where the EGCC is relatively more slope-controlled: the ratio $A_{on}/A_{off} \approx 1$, compared to $A_{on}/A_{off} << 1$ at all other JR105 locations (excluding section 5). Overall, the predicted scales match the observations quite well, suggesting that the dynamics of the EGCC may be appropriately described by the theoretical ideas developed previously for smaller scale buoyant flows.

5.2 Wind forcing

To examine the role of wind on forcing the EGCC, we regressed the alongshelf wind stress, τ_{along}, versus four variables: the observed depth (h_{obs}) and width (w_{obs}) scales of the EGCC, and the absolute volume and freshwater fluxes for each year. These regressions, which are based on the summertime data taken near Cape Farewell over the years 1997-2004 described above, are shown in Figs. 13 and 14. Wind stresses were calculated from the twice-daily QuikSCAT scatterometer wind fields using a drag formula (Large and Pond, 1981), and rotated into along- and cross-shelf components. We define τ_{along} as the average over the two days prior to the time of completion of the CTD section. This averaging time scale was chosen for several reasons. First, the CTD sections generally took 1-2 days to complete. Second, two days is the amount of time it would take an offshore Ekman flux driven by a 0.1 N/m^2 wind stress to move the entire area of water present on the shelf near Cape Farewell off the shelf. Essentially, this timescale is equivalent to the wind strain timescale that Whitney and Garvine (2005) derived, and over which winds must blow to significantly influence a buoyant plume's density structure. Lastly, two days is roughly the decorrelation time scale of the winds estimated at Cape Farewell with QuikScat data for the year 2004. Note that this averaging reduces the magnitude of the wind stresses in Figures 13 and 14, while in fact the maximum wind

stresses during storm events in summer can exceed 0.2 N/m^2 (corresponding to wind speeds in excess of 20 m/s).

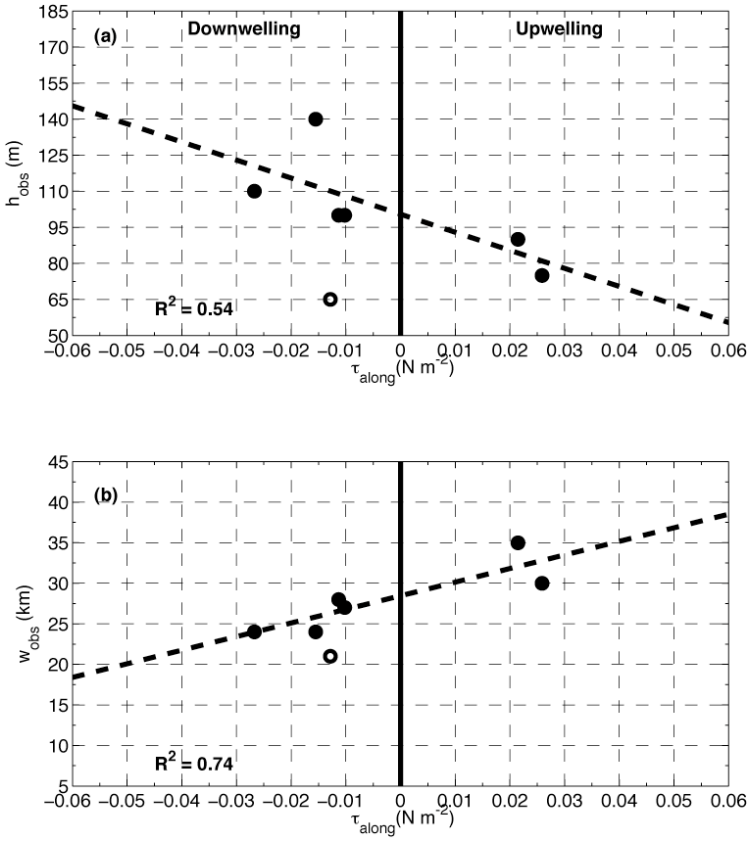

Figure 13. *(a)* Depth of the 34-isohaline at the bottom, h_{obs}, which indicates the foot of the EGCC front at Cape Farewell, as a function of alongshelf wind stress (upwelling favorable: $\tau_{along} > 0$). The dashed line is a linear fit to the Cape Farewell data. Open circles were not used in the regression (see text). *(b)* Same as Fig. 13a, except for the width of the EGCC, w_{obs}, versus τ_{along}.

The regressions in Figs. 13 and 14 suggest that the EGCC is responding to the alongshelf wind stress qualitatively akin to what has been observed for smaller scale coastal currents at mid-latitudes. For downwelling wind, $\tau_{along} < 0$, the depth of the front increases, the current narrows, and the equatorward volume transport increases. The anomalous h_{obs} observed in 2003 was excluded from the depth correlation. Choosing an isohaline that captures the EGCC in 2003, such as $S = 34.5$, and then calculating h_{obs}, would have corrected the observed depth to be in line with the rest of the data, but to be consistent we used the same definition for all years and excluded the 2003 data from all the correlations. A more sophisticated method may be useful in the future. Note that the freshwater flux was not significantly correlated with the wind stress (the remaining

regressions were significant at the 95% level), implying the importance of the salinity field to the FW_{flux} calculation. If no low-salinity water is present at the time, the FW_{flux} will not increase substantially even if strong downwelling favorable winds are blowing.

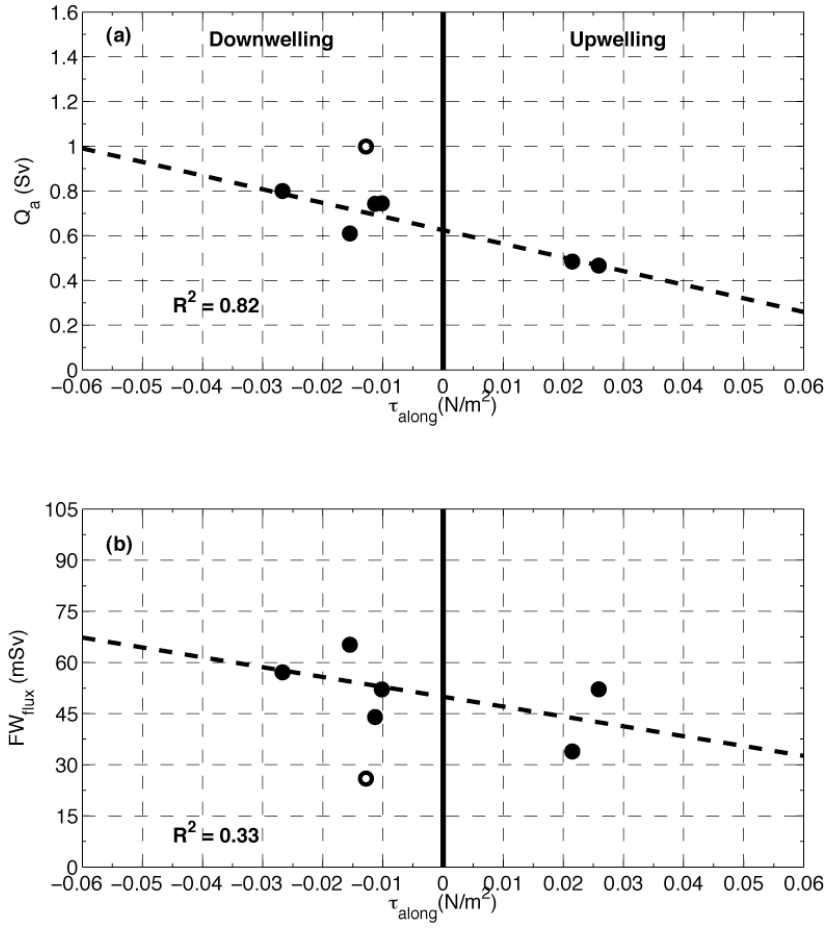

Figure 14. *(a)* Same as Fig. 13a, except for EGCC absolute transport, Q_a, versus τ_{along}. The linear fit is used to adjust the JR105 transports into "no-wind" values as discussed in the text. *(b)* Same as Fig. 13a, except for EGCC freshwater flux, FW_{flux}, versus τ_{along}.

The total observed ranges for h_{obs}, w_{obs}, and Q_a are: a deepening of 75 m, a narrowing of 20 km, and an increase in transport of 0.5 Sv. Clearly the EGCC varies substantially with the wind. Are such wind events strong enough to reverse the coastal current? We can check this by applying the wind strength index (W_s) discussed above to each crossing. This was done using the observed scales of the EGCC shown in Fig. 3-7 and Fig. 10-12. To estimate the wind-driven velocity scale, we follow Whitney and

Garvine (2005) who use quadratic drag laws to represent the surface and bottom stresses resulting in the simple expression

$$u_{wind} = \sqrt{\frac{\rho_{air}}{\rho}\frac{C_{10}}{C_D}} \cdot U \approx 2.65 \times 10^{-2} \cdot U \quad (4)$$

where ρ_{air} is the air density, ρ is the water density, C_{10} is the surface drag coefficient, C_D is the bottom drag coefficient, and U is the wind velocity. The buoyant velocity scale can be estimated by considering a two-layer thermal wind balance where the lower layer is at rest and the upper layer is of thickness h_{obs}. This gives the scale

$$u_{buoy} = \left(\frac{\sqrt{g' h_{obs}}}{f \cdot w_{obs}}\right)\left(2 g' Q_a f\right)^{1/4} \quad (5)$$

where the first factor is the Rossby radius of deformation, $R = (g'h_{obs})^{1/2}/f$, divided by the current width, and the second factor includes the reduced gravity, the transport, and the Coriolis parameter, representing a gravity current speed $(g'h_{obs})^{1/2}$.

Taking U in (4) to be the same wind velocity used to calculate the wind stresses, the corresponding values of W_s for the EGCC at Cape Farewell are listed in Table 1, and the values for the remaining 2004 sections in Table 2. Note that $|W_s| < 1$ for all years and sections. This implies that the EGCC is always in a buoyancy-driven state, at least for the times that observations exist. This is consistent with the results of Whitney and Garvine (2005) who showed that for a larger scale coastal current such as the Alaska Coastal Current, strong wind events did not result in wind-driven flow reversals that occur for smaller scale currents such as the Delaware River Coastal Current. The largest $|W_s|$ occurred in 2003 due to the decreased stratification and relatively high wind speeds; the largest positive W_s occurred during JR105 at section 5 where the strongest upwelling winds were recorded and the EGCC is the least well-defined.

The 2004 Cape Farewell section is notable as having the largest positive W_s at that location, suggesting that it was during this occupation that the wind had the strongest effect on the EGCC structure and flow. Given the same stratification, transport, and structure of the EGCC, U would need to be ~27 m/s in order for W_s to be O(1). These are strong winds, but not unreasonable for a storm event. In contrast, given a weaker stratification, such as for OC395 in 2003 where g' was less than one third its 2004 value, less intense winds, on the order of ~18 m/s, could potentially reverse the EGCC flow. Wintertime might be the season for such flow reversals, since the winds are stronger and without any sea ice melt the stratification is lower.

6 Adjusted alongstream trends of the EGCC/EGC system

Using the regression line of Fig. 14a, we can determine an undisturbed (no wind) value of Q_a for the EGCC at Cape Farewell, which is 0.66 Sv. Furthermore, we can calculate a percentage increase (decrease) for the transport as the wind stress becomes increasingly downwelling favorable, $\tau_{along} < 0$ (upwelling favorable, $\tau_{along} > 0$). If we assume that the same relationship holds for all latitudes during JR105, we can adjust the volume transports at each section for the wind stress observed there. For example, at section 2 the observed transport was 2.2 Sv with a two-day average wind stress of -0.028 N/m^2. Since the winds were downwelling favorable, the adjusted transport will be smaller, in this case equal to 1.54 Sv (a 33% decrease).

This approach is an empirical one that differs from previous attempts to estimate the wind's effect on the buoyant current transport (Whitney and Garvine, 2005; Lentz and Largier, 2006). In those studies, the transport is assumed to be linear and is decomposed into wind-driven and buoyancy-driven components that can be estimated separately. The critical assumption is that the winds force a barotropic response that does not affect the density driven flow significantly. This assumption has drawbacks, most notably that any barotropic response will result in a set-up or set-down that will drive a geostrophic response. Our approach is strictly observational and hence accounts for such feedbacks. Admittedly, however, the range of observed winds in our study is limited, with only two upwelling events.

Adjusting the EGCC transports for the observed winds during JR105 results in the alongstream transport trend shown in Fig. 8a (solid, thick gray line). The most dramatic change occurs at section 2 where the anomalous increase in transport is partially reduced. However, when the adjusted EGCC transport values are combined with the transports of the EGC (solid, thick black line in Fig. 8a), we find that the jump noted previously at section 2 is completely removed. In the adjusted case, the combined EGCC/EGC system has a nearly constant volume transport of 2 Sv along the entire southeast coast of Greenland. This means that, as a combined current system, the volume transport trend is consistent with there being no sources or sinks of mass.

Performing the analogous adjustment to the EGCC freshwater fluxes, we find that the alongstream trend in FW_{flux} is also significantly altered. Instead of showing a large increase from section 5 to section 2, followed by a substantial drop from section 2 to

section 1 at Cape Farewell, the adjusted FW_{flux} increases more slowly to section 2 and does not drop off by as much at Cape Farewell. A more dramatic change occurs in the combined EGCC/EGC system where now the FW_{flux} increases equatorward from 55 mSv at section 5 to 103 mSv at section 2, then stays roughly constant to Cape Farewell. This estimate at section 2 (and section 1) is similar to the estimate for the combined EGCC/EGC system computed by Dickson et al. (2007) for the southeast Greenland shelf. The overall increase in the adjusted FW_{flux} along the path of the EGCC/EGC is approximately 38 mSv, very close to the net gain seen in the original values, but the changes from section to section differ substantially. This adjusted trend seems to make more intuitive sense for a region accumulating freshwater along its entire path.

7 Freshwater budget

South of Denmark Strait, the EGC and EGCC are the only surface pathways of low-salinity water and hence play a major role in controlling the freshwater distribution in the western North Atlantic. Beyond Cape Farewell, part of the flow of the West Greenland Current eventually joins the Labrador Current and carries this fresh signal all the way to the Middle Atlantic Bight (Fratantoni and Pickart, 2007). The pathway from the Labrador Sea to the Middle Atlantic Bight has been studied more extensively (e.g., Loder et al., 1998), yet the freshwater pathways on the southeast Greenland shelf, which feed into this larger scale system, have not been detailed.

Four freshwater sources could potentially alter the FW_{flux} along the EGC/EGCC pathway. The total FW_{flux} is the sum of these sources, plus advection:

$$FW_{flux} = FW_{adv} + FW_{seaice} + FW_{iceberg} + FW_{runoff} + FW_{PE} \quad (6)$$

where FW_{adv} is the freshwater advected through the system, FW_{seaice} is the meltwater from sea ice, $FW_{iceberg}$ is the meltwater from icebergs calved off Greenland, FW_{runoff} is the runoff from Greenland that is mainly meltwater, and FW_{PE} is the net precipitation minus evaporation (P-E) over the area. By not accounting for the temporal or spatial variability of each source term in (6), we are essentially assuming that the total annual mean value was available to the EGCC/EGC system during JR105 and that the distribution is linear along the shelf. Each source term has large natural variability and a considerable range of values are found in the literature. However, the added complexity of addressing such variability is not warranted for the rough budget considered here.

Fig. 15 displays the net freshwater gain estimated for the Greenland shelf from

68°N to 60°N. The largest contribution comes from the melting of sea ice, which is advected from the Arctic Ocean through Fram Strait, then Denmark Strait, and melts along its way during summer. By the latitude of Cape Farewell, no significant sea ice concentration is typically observed in late summer, so any ice at Denmark Strait must melt during its transit down the shelf in the EGC/IC and EGCC. No previous study has directly estimated the volume of ice flux leaving the Nordic Seas through Denmark Strait. As a remnant inflow of Fram Strait ice, the ice flux farther south is usually approximated by looking at the reduction in ice extent. Aagaard and Carmack (1989) used a flux of 18 mSv based on ice extent maps, while more recent satellite imagery implies a flux of 19 mSv (assuming 75 mSv as a best guess for the Fram Strait flux, Kwok and Rothrock, 1999). From Denmark Strait to Cape Farewell then, ~19 mSv is available to the EGC and EGCC. Whether or not all of this freshwater enters into the currents or stays with them along the entire path is another question; this value represents an upper bound.

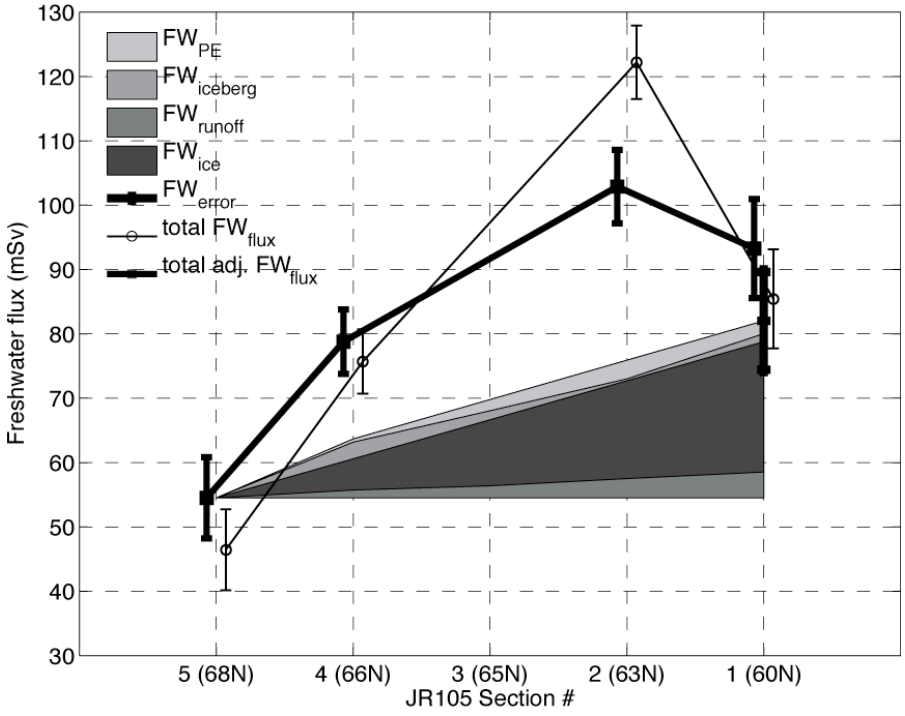

Figure 15. The trend in freshwater flux, FW_{flux} (mSv, referenced to S_{ref} = 34.8), for the EGC/EGCC system along the East Greenland shelf from 68°N to 60°N, showing the wind-adjusted (bold line) and original (thin line) values. Shading indicates the freshwater sources (iceberg calving and melt, sea ice melt, net P–E, and meltwater runoff) available to the EGC/EGCC system assuming the section 5 FW_{flux} as a starting point.

The remaining three source terms are all the same order of magnitude, and are all significantly less than the sea ice melt term. Runoff from Greenland is mainly meltwater and not riverine. There are specific high output areas, such as at the mouth of the Kangerdlugssuaq Trough (Fig. 1), but for our purposes we take the cumulative input of meltwater along the coastal area and ignore spatial variability. The estimate of 4 mSv is taken from a surface mass balance calculation using a regional climate model of the Greenland continent, then summed over the JR105 area, 68°N to 60°N (Box et al., 2006; Box et al., 2004). Evidence of increased melt and enhanced thinning of ice along the Greenland coast is mounting (Krabill et al., 2004; Krabill et al., 1999), yet the increased freshwater input would be insignificant compared with the errors in this rough freshwater budget.

Solid ice, in the form of icebergs, also originates from the Greenland continent and subsequently melts in the shelf waters. Estimates of iceberg calving rates for this region vary from 1.5 mSv (Rignot et al., 2004) to 2.7 mSv (Bigg, 1999). Since most of this ice will melt by Cape Farewell, we assume the additional freshwater available to the shelf area equals the iceberg calving rate and use 2 mSv as our best estimate in Fig. 15. P-E over the Greenland continent is taken into account in the runoff term, while precipitation rates near the Greenland coast have a large range. Next to the coast orographic effects can increase yearly values to >2 m/yr, while over much of the shelf values are ~0.3 m/yr (Box et al., 2004). We estimate a net P-E of 2.5 mSv using those values and an area of 1.5 x 10^5 km^2 for the shelf from 68°N to 60°N (depth < 400m).

Cumulatively, these freshwater sources represent an addition of 27.5 mSv to the EGC/EGCC system. This is the right magnitude to account for the observed net (wind-adjusted) FW_{flux} increase of 38 mSv, since calculated error estimates are on the order of ±7-10 mSv.

8 Discussion

Although we have shown that the EGCC is present along the entire southeast Greenland coast in summer and that a consistent freshwater budget for the adjoining shelf region can be constructed, a compelling open question remains: What explains the large transport and length scales of the EGCC on the inner shelf if it is not purely meltwater driven? In other words, what is the origin of the EGCC? We believe that it forms due to a bifurcation of the EGC south of Denmark Strait. Note that only a weak EGCC was

observed on the shelf north of Denmark Strait (Fig. 7), and a coastal current has never been previously reported farther north on the Greenland shelf (albeit that region is very difficult to observe). Also, the θ/S properties of the EGCC closely follow those of the EGC observed at Denmark Strait, suggesting a shared Arctic source (Fig. 2). Additional confirmation of a common source is provided by the nutrient and oxygen isotope data collected during JR105 (see Sutherland et al., 2008).

By what mechanism does the EGC bifurcate? Canyons and bathymetric bends have been shown to strongly influence buoyant coastal currents, though the exact behavior depends on the degree of the bathymetric anomaly, the stratification, and the strength of any ambient flow (Williams et al., 2001; Chapman, 2003; Wolfe and Cenedese, 2006). One such bathymetric effect is the separation of a buoyant current across a gap if it is unable to navigate the canyon. We hypothesize that some portion of the EGC is diverted onto the shelf in this manner when the current encounters the wide (50 km) and deep (> 200 m) KG trough. Upstream of JR105 section 4, the water in the vicinity of the trough is anomalously warm (T ~ 6-7°C, Fig. 9b) and salty (S > 32.5) compared to the surrounding shelf water (T ~ 4-5°C, S < 32.5). This implies that part of the EGC turns inshore here, carrying with it warmer and saltier Atlantic-origin water from the shelfbreak. This is consistent with an XCTD section (not shown) occupied in 2002 which indicates the presence of AW on both sides of the trough, while the center of the trough contains colder and fresher water. Sea ice concentrations observed remotely from the SMMR and SSM/I instruments are consistent with this notion as well (Cavalieri et al., 2005). On the other hand, the tracer measurements of Pickart et al. (2005) suggest that the EGC can also take a more direct route along the shelfbreak at the seaward edge of the KG trough. This implies that there may be a time-dependent bifurcation of the flow associated with the anomalous bathymetry of the KG.

Once the flow is diverted onshore, it is still not obvious why it should remain on the inner shelf (versus flowing back offshore along the western side of the KG trough). There are at least two possibilities. The first is associated with the diverging isobaths on the western side of the head of the KG, which may lead to a splitting of the flow as it crosses the head of the trough. This would form an inner branch near the coast and a return branch that flows back to the shelfbreak. A second potential mechanism involves mixing within the canyon, possibly induced by local eddy formation. Such mixing would

alter the stratification, which in turn would impact the trapping depth of the buoyant flow possibly allowing it to cross isobaths and emerge as an inner branch.

Regardless of the precise cause, our observations show that the EGCC exists equatorward of the KG, and that it undergoes additional modification downstream as it receives meltwater runoff and sea ice melt. The two branches (EGC and EGCC) come in close proximity again near JR105 section 2 (63°N) where the shelf narrows to less than 40 km. South of this latitude the bathymetry again seems to influence the circulation, where much of the flow is diverted offshore to rejoin the EGC/IC system at the shelfbreak. This offshore movement is most likely due to a basin feature on the shelf located just downstream of section 2, an idea supported by the drifter data of Reverdin et al. (2003) and Jakobsen et al. (2003). Fig. 16 summarizes schematically the overall coastal circulation along southeast Greenland implied by the JR105 measurements, including the apparent effect of bathymetry on the paths of the EGCC and EGC.

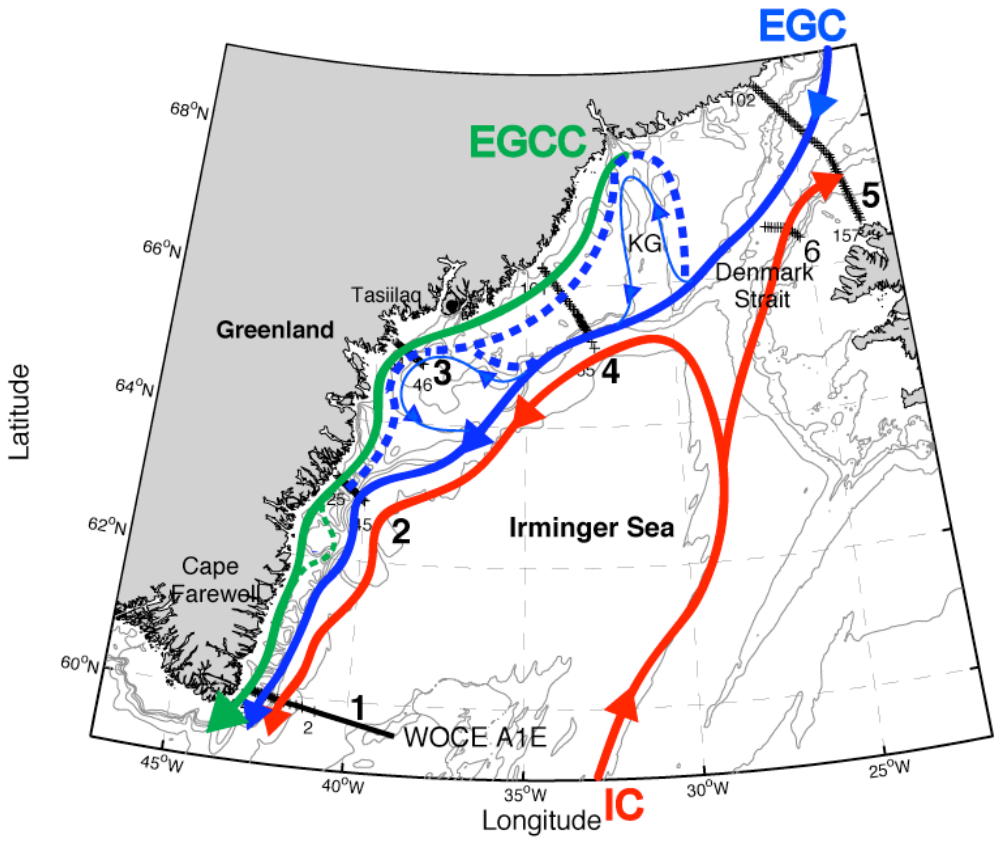

Figure 16. Surface circulation schematic for the summertime boundary current system of the Irminger Sea. Solid lines show observed paths of the EGC, EGCC, and the IC, while dashed lines indicate possible flow paths induced by bathymetric or wind effects. North of the KG trough the EGCC's presence is uncertain, though it is likely weaker than what is observed farther south.

9 Conclusions

We have presented the first comprehensive description of the East Greenland Coastal Current (EGCC) on the southeast Greenland shelf, primarily using measurements from a hydrographic/velocity cruise conducted in summer 2004. It was demonstrated that the EGCC exists along the entire 1000 km long shelf, distinct from the shelfbreak flow of the East Greenland Current (EGC), with a high velocity core (ranging from 50-100 cm/s) and a characteristic low-salinity, wedge-shaped structure. The single exception to this was near 63°N, where the shelf narrows considerably and the EGC comes into close proximity with the EGCC. This merging of the two currents, when added to the evidence of the EGC bifurcation farther upstream inferred from θ/S measurements, satellite sea ice data, and previous drifter studies, suggests that the EGCC is an inner branch of the EGC. Correspondingly, any accounting of the volume and freshwater budgets of the Irminger Sea region must include the EGC and EGCC as an integrated system.

Indeed, we find that when considered together, the EGC/EGCC transports co-vary, carrying a relatively constant 2 Sv of water equatorward along the shelf. This trend emerged only after the effect of alongshelf winds was considered; the significant variability observed in the EGCC hydrographic and velocity structure at each section is related in part to the strength of the alongshelf wind stress, with downwelling favorable winds corresponding to higher transports, and a deeper, narrower EGCC. The net gain in freshwater transport of the combined EGCC/EGC system from Denmark Strait to Cape Farewell, adjusted for the response to alongshelf wind stress, was 38 ± 9.9 mSv. This compares favorably to the magnitude of available freshwater from melting of sea ice and icebergs, meltwater runoff from Greenland, and net P-E. Together, these sources can add about 27.5 ± 7.5 mSv to the shelf area during the year. Overall, the volume and freshwater transport trends display a more interpretable trend when the EGCC and EGC are considered as a composite system.

More long term measurements of the EGCC, and the entire shelf circulation, will answer many of the questions raised in this paper on the temporal and spatial variability of the EGCC. Obtaining a clearer understanding of how freshwater is distributed in the subpolar North Atlantic is essential to establish a baseline of knowledge in this climate-sensitive area of the world's oceans.

Acknowledgments

The authors would like to thank T. McKee for calibration of the hydrographic data and other data processing, D. Torres for the processing of the ADCP data, and P. Fratantoni for help in the ADCP stream coordinate transformation. Many thanks also go to the captain and crew of the *RRS James Clark Ross*. This work was funded by the National Science Foundation grant OCE-0450658. DS was also partially supported by the Woods Hole Oceanographic Institution Academic Programs Office.

References

Aagaard, K. and E. C. Carmack (1989). The role of sea ice and other fresh water in the Arctic circulation. *Journal of Geophysical Research*, **94,** 14485-14498.

Bacon, S., G. Reverdin, I. G. Rigor, and H. M. Smith (2002). A freshwater jet on the east Greenland shelf. *Journal of Geophysical Research*, **107,** doi:10.1029/2001JC000935.

Bigg, G.R. (1999). An estimate of the flux of iceberg calving from Greenland. *Arctic, Antarctic, Alpine Research*, **31**, 174-178.

Box, J.E., D.H. Bromwich, and L.-S. Bai (2004). Greenland ice sheet surface mass balance 1991-2000: application of Polar MM5 mesoscale model and in situ data. *Journal of Geophysical Research*, **109,** doi:10.1029/2003JD004451.

Box, J.E., et al. (2006). Greenland ice sheet surface mass balance variability (1988-2004) from calibrated Polar MM5 output. *Journal of Climate*, in press.

Bryan, F. (1986). High-latitude salinity effects and interhemispheric thermohaline circulations. *Nature*, **323,** 301-304.

Cavalieri, D., C. Parkinson, P. Gloerson, and H.J. Zwally (2005). Sea ice concentrations from Nimbus-7 SMMR and DMSP SSM/I passive microwave data, 2001-2004. Boulder, CO, USA: National Snow and Ice Data Center.

Clarke, R.A. (1984). Transport through the Cape Farewell-Flemish Cap section. *Rapp. P.-v.Reunn. cons. int. Explor. Mer.*, **185**, 120-130.

Curry, R., R. R. Dickson, and I. Yashayaev (2003). A change in the freshwater balance of the Atlantic Ocean over the past four decades. *Nature*, **426,** 826-829.

Dickson, R., B. Rudels, S. Dye, M. Karcher, J. Meincke, and I. Yashayaev (2007). Current estimates of freshwater flux through Arctic and subarctic seas. *Progress in Oceanography,* **73***,* 210-230.

Egbert, G.D., A.F. Bennett, and M.G.G. Foreman (1994). TOPEX/POSEIDON tides estimated using a global inverse model. *Journal of Geophysical Research*, **99**, 24821-24852.

Fong, D.A., W.R. Geyer, and R.P. Signell (1997). The wind-forced response of a buoyant coastal current: observations of the western Gulf of Maine plume. *Journal of Marine Systems*, **12,** 69-81.

Fong, D.A. and W.R. Geyer (2001). Response of a river plume during an upwelling favorable wind event. *Journal of Geophysical Research*, **106,** 1067-1084.

Fratantoni, P.S., R.S. Pickart, D.J. Torres, and A. Scotti (2001). Mean structure and dynamics of the shelfbreak jet in the Middle Atlantic Bight during fall and winter. *Journal of Physical Oceanography*, **31**, 2135-2156.

Fratantoni, P.S., and R.S. Pickart (2007). The Western North Atlantic shelfbreak current system in summer. *Journal of Physical Oceanography,* **37***,* 2509-2533.

Halkin, D., and T. Rossby (1985). The structure and transport of the Gulf Stream at 73W.

Journal of Physical Oceanography, **15**, 1439-1452.
Hansen, B. and S. Østerhus (2000). North Atlantic-Nordic Sea exchanges. *Progress in Oceanography*, **45**, 109-208.
IOC, IHO and BODC (2003). Centenary Edition of the GEBCO Digital Atlas, published on CD-ROM on behalf of the Intergovernmental Oceanographic Commission and the International Hydrographic Organization as part of the General Bathymetric Chart of the Oceans, British Oceanographic Data Centre, Liverpool, U.K.
Jakobsen, P.K., M.H. Ribergaard, D. Quadfasel, T. Schmith, and C.W. Hughes (2003). Near-surface circulation in the northern North Atlantic as inferred from Lagrangian drifters: variability from the mesoscale to the interannual. *Journal of Geophysical Research,* **108**, doi:10.1029/2002JC001554.
Krabill, W., et al. (1999). Rapid thinning of parts of the southern Greenland ice sheet. *Science*, **283**, 1522-1524.
Krabill, W., et al. (2004). Greenland Ice Sheet: increased coastal thinning. *Geophysical Research Letters.*, **31**, doi:10.1029/2005GL021533.
Krauss, W. (1995). Currents and mixing in the Irminger Sea and in the Iceland Basin. *Journal of Geophysical Research*, **100**, 10851-10871.
Kwok, R. and D. A. Rothrock (1999). Variability of Fram Strait ice flux and the North Atlantic Oscillation. *Journal of Geophysical Research*, **104**, 5177-5189.
Large, W.G., and S. Pond (1981). Open ocean momentum flux measurements in moderate to strong winds. *Journal of Physical Oceanography*, **11**, 324-336.
Lentz, S.J. and J. Largier (2006). The influence of wind forcing on the Chesapeake Bay buoyant coastal current. *Journal of Physical Oceanography*, **36**, 1305-1316.
Loder, J.W., B. Petrie, and G. Gawarkiewicz (1998). The coastal ocean off northeastern North America. A large scale view. in *The Sea*, A.R. Robinson and K.H. Brink, Eds., 105-153.
Malmberg, S-A., H.G. Gade, and H.E. Sweers (1967). Report on the second joint Icelandic-Norwegian expedition to the area between Iceland and Greenland in August-September 1965. *NATO Subcommittee on Oceanographic Research*, Technical Report No. 41, Irminger Sea Project, 44 pp.
Melling, H. (2000). Exchanges of freshwater through the shallow straits of the North American Arctic. *The freshwater budget of the Arctic Ocean*, E. E. Lewis, Ed., Kluwer, 479-502.
Mork, M. (1981). Circulation phenomena and frontal dynamics of the Norwegian Coastal Current. *Philosophical Transactions of the Royal Society of London*, *Series A*, **302**, 635-647.
Nilsson, J., G. Bjork, B. Rudels, P. Winsor, and D. Torres (2006). Late-winter conditions and freshwater transport in the East Greenland Current: results from an icebreaker-based survey. *Journal of Geophysical Research,* submitted.
Pickart, R.S., D.J. Torres, and P.S. Fratantoni (2005). The East Greenland spill jet. *Journal of Physical Oceanography*, **35**, 1037-1053.
Reverdin, G., P.P. Niiler, and H. Valdimarsson (2003). North Atlantic Ocean surface currents. *Journal of Geophysical Research*, **108**, doi:10.1029/2001JC001020.
Rignot, E., D. Braaten, S.P. Gogineni, W.B. Krabill, and J.R. McConnell (2004). Rapid ice discharge from southeast Greenland glaciers. *Geophysical Research Letters*, **31**, doi:10.1029/2004GL019464.
Rudels, B., E. Fahrbach, J. Meincke, G. Budeus, and P. Eriksson (2002). The East Greenland Current and its contribution to the Denmark Strait overflow. *ICES Journal of Marine Science*, **59**, 1133-1154.
Sutherland, D.A. (2008). The East Greenland Coastal Current: its structure, variability,

and large-scale impact. PhD thesis, MIT/WHOI Joint Program, 161 pp.
Sutherland, D.A., R.S. Pickart, E.P. Jones, K. Azetsu-Scott, A.J. Eert, and J. Ólafsson (2008). Freshwater composition of the waters off southeast Greenland and their link to the Arctic Oscillation. *Journal of Geophysical Research*, Submitted.
Weingartner, T.J., S. Danielson, Y. Sasaki, V. Pavlov, and M. Kulakov (1999). The Siberian Coastal Current: A wind- and buoyancy forced Arctic coastal current. *Journal of Geophysical Research*, **104**, 29697-29713.
Weingartner, T.J., Danielson S.L. and T.C. Royer (2005). Freshwater variability and predictability in the Alaska Coastal Current. *Deep-Sea Research II*, **52**, 169-191.
Wilkinson, D. and S. Bacon (2005). The spatial and temporal variability of the East Greenland Coastal Current from historic data. *Geophysical Research Letters*, **32**, doi:10.1029/2005GL024232.
Williams, W.J., G. Gawarkiewicz, and R.C. Beardsley (2001). The adjustment of a shelfbreak jet to cross-shelf topography. *Deep-Sea Research II*, **48**, 373-393.
Wolfe, C.L., and C. Cenedese (2006). Laboratory experiments on eddy generation by a buoyant coastal current flowing over variable bathymetry. *Journal of Physical Oceanography*, **36**, 395-411.
Woodgate, R.A. and K. Aagaard (2005). Revising the Bering Strait freshwater flux into the Arctic Ocean. *Geophysical Research Letters*, **32**, L02602, doi:10.1029/2004GL021747.
Yankovsky, A.E. and D.C. Chapman (1997). A simple theory for the fate of buoyant coastal discharges. *Journal of Physical Oceanography*, **27**, 1386-1401.